RESEARCH Open Access



5.2-THz-bandwidth miniaturized spectrometer using a GHz-tunable laser

Huashan Yang^{1†}, Xiaohu Tang^{1†}, Hao Zhang^{1†}, Lihan Wang¹, Zongxin Ju¹, Zhe Kang¹, Jijun He^{1*} and Shilong Pan^{1*}

[†]Huashan Yang, Xiaohu Tang and Hao Zhang contributed equally to this work.

*Correspondence: jijun.he@nuaa.edu.cn; pans@nuaa.edu.cn

1 National Key Laboratory of Microwave Photonics, Nanjing University of Aeronautics and Astronautics, Nanjing 210016, China

Abstract

The increasing demand for dispersion engineering in various photonic applications necessitates spectrometry with both kilohertz resolution and several terahertz bandwidth. A laser with sufficiently large frequency tuning range is required in traditional methods, Yielding bulky and expensive systems that are difficult to integrated on a chip. Compact, high-resolution, and broadband spectrometers are crucial, yet onchip integration, particularly of the optical source, remains challenging. Here, we propose a 5.2-THz-bandwidth miniaturized spectrometer utilizing a laser only in GHz tuning range. The laser's tuning range is leveraged by integrated Si₃N₄ soliton microcombs to achieve a 650-times larger measurement bandwidth, extending the measurement range from 1525.3 to 1566.8 nm and surpassing the optical C-band. The soliton microcomb is meticulously frequency-stabilized, achieving frequency fluctuations below 100 Hz, ensuring high frequency precision for our spectrometer. By combining optical asymmetrical double sideband modulation with soliton microcombs, we significantly enhance the spectrometer's performance, offering higher resolution, larger dynamic range, and greater bandwidth. This optical spectrum measurement approach enabled by GHz-tunable laser opens a way to significantly simplify system complexity.

Keywords: Spectroscopy, Frequency comb, Soliton microcomb, Microwave photonics, Integrated photonics

Introduction

Recent developments in optical devices and applications, including integrated optical components [1], high-Q optical micro-resonators [2, 3], optical nanoparticle detection [4], and molecular spectroscopy [5], present unprecedented demands for both bandwidth and frequency resolution in measurements. Particularly in dispersion engineering, which is indispensable in many fields, such as mode-locked laser [6], metasurface [7], optical supercontinuum generation [8], photonic parametric amplifier [9], Kerr optical frequency comb [10–13], and so on, spectrometry with simultaneous kilohertz resolution and several terahertz bandwidth is imperative. Dual-comb spectroscopy (DCS) [14, 15] is a promising solution that offers high resolution and wide bandwidth. However, it typically requires complex stabilization schemes and high system costs due to the need for mutual coherence between two combs. To date, the most common method for



© The Author(s) 2025. **Open Access** This article is licensed under a Creative Commons Attribution 4.0 International License, which permits use, sharing, adaptation, distribution and reproduction in any medium or format, as long as you give appropriate credit to the original author(s) and the source, provide a link to the Creative Commons licence, and indicate if changes were made. The images or other third party material in this article are included in the article's Creative Commons licence, unless indicated otherwise in a credit line to the material. If material is not included in the article's Creative Commons licence and your intended use is not permitted by statutory regulation or exceeds the permitted use, you will need to obtain permission directly from the copyright holder. To view a copy of this licence, visit http://creativecommons.org/licenses/by/4.0/.

Yang et al. PhotoniX (2025) 6:32 Page 2 of 14

broadening the measurement bandwidth is to sweep the wavelength of tunable external cavity diode lasers (ECDLs) [16–26]. However, high-performance ECDLs with narrow linewidths, wide wavelength tuning ranges, and high wavelength precision are typically bulky and expensive. Additionally, complex frequency calibration is inevitable in wavelength scanning schemes [16, 17], and the optical linewidth may deteriorate during the scanning process [16].

Microwave photonics [27, 28] emerges as a potent tool for measuring optical spectral responses. Recent developments [19-25, 29] indicate that the resolution of electrooptical modulation-based spectrometers can reach levels comparable to the linewidths of optical sources because microwave signals usually have much smaller linewidths than optical sources. In addition to traditional transmission measurements, microwave photonic optical vector analysis enables phase measurement for the optical devices. Among these methods, optical double-sideband modulation [24, 25, 29] based spectrometers offer doubled channel bandwidth compared to single-sideband modulation and remain unaffected by residual opposite sidebands. Despite the ultra-high resolution achieved in [29], the use of narrowband EO-combs with poor flatness limits the measurement bandwidth. Furthermore, non-flat comb lines in EO-combs introduce unavoidable residual noises from other channels, degrading the accuracy of the measurement. Amidst the growing demand for miniaturized spectrometers, preliminary research using an ECDL has suggested the feasibility of integrated spectrometers [22]. However, the journey towards achieving small size and portability while maintaining high-performance broadband spectrometers remains challenging.

In this work, we introduce a miniaturized, high-precision, broadband spectrometer that distinctively utilizes a GHz-tunable laser. The optical spectrum of the laser is broadened by an integrated Si₃N₄ dissipative Kerr soliton (DKS) optical frequency comb, also known as a soliton microcomb. This broadening Yields an exceptionally high measurement bandwidth ranging from 1525.3 to 1566.8 nm, extending beyond the optical C-band. The measurement bandwidth is significantly improved by 650 times compared to the laser's electrical frequency tuning range. Through leveraging the versatile merits of soliton microcombs, we effectively address the limitations encountered in our previous work [29]. Over the past decade, integrated soliton microcombs have shown excellent performance, with low noise, wide bandwidth, and a tunable FSR from gigahertz to terahertz [10-12, 30-33]. These features make them useful in many areas [34], such as high-speed optical communication [35-37], ultrafast and long-distance ranging [38-40], dual-comb spectroscopy [41-43], astronomical spectrometer calibration [44], optical neural network [45, 46], signal processing [47-50], and microwave synthesis [51, 52]. By leveraging the broad, flat, and low-noise spectrum of soliton microcombs, this study extends the measurement bandwidth of our spectrometer to 5.2 THz (equivalent to a 41 nm span in the C band), concurrently improving the signal-to-noise ratio (SNR) of the system. The precision of the spectrometer is meticulously maintained through the employment of optical frequency stabilization, achieving a frequency fluctuation below 100 Hz, ensuring high precision for the proposed spectrometer. The frequency resolution is better than 10 kHz due to the narrow linewidth feature of soliton microcomb [53]. Combining the high-resolution, high dynamic range, and doubled channel bandwidth exceeding 100 GHz attributes of the optical asymmetrical double sideband (DSB)

Yang et al. PhotoniX (2025) 6:32 Page 3 of 14

modulation method with the soliton microcomb's capabilities result in significantly streamlined and enhanced spectrometer performance. The soliton microcomb with large FSR perfectly matches the asymmetrical DSB method's channel bandwidth, minimizing the influence of channel switching. This innovative approach, relying solely on a GHz-tunable laser, not only simplifies the complexity and reduces the size of our spectrometer but also substantially boosts its performance, marking a significant advancement in optical measurements.

Generation and Stabilization of the soliton microcomb

The soliton microcomb is generated by pumping a Si₃N₄ micro-resonator with a 1550 nm continuous-wave (CW) laser (NKT Koheras ADJUSTIK E15), which is amplified by an Erbium-doped fiber amplifier (EDFA1), as shown in Fig. 1(a). The Si₃N₄ microresonator, fabricated on 800 nm thick Si_3N_4 , has a Q-factor of 3×10^6 and an FSR of 103.9 GHz. The CW laser has a thermal tuning range of approximately 1 nm, which is utilized for aligning the laser frequency with the resonance of the Si₃N₄ micro-resonator. Note that once frequency alignment is achieved, the thermal frequency tuning is no longer activated. The soliton microcomb is then generated using only the 8 GHz electrical tuning range of the CW laser, which is extremely narrow-650 times smaller than the bandwidth required for our broadband spectrometer. This GHz-level tuning range is required for soliton generation using the forward and backward tuning technique [54]. However, if the self-injection locking technique [55] is employed, the need for such GHz-range tuning can be eliminated. To mitigate the amplified spontaneous emission (ASE) noise from the pump laser, an optical bandpass filter (OBPF1) is employed. Subsequently, a tunable fiber Bragg grating (FBG) is used to suppress the residual pump line in the output optical spectrum. Following the generation of the single-soliton microcomb, stabilization processes for the frequency of the comb lines are implemented, as illustrated in Fig. 1. These processes enhance the stability of the comb line frequencies, providing a precise and stable optical source for the proposed spectrometer. With the aid of two optical filters, a sech²-shaped soliton

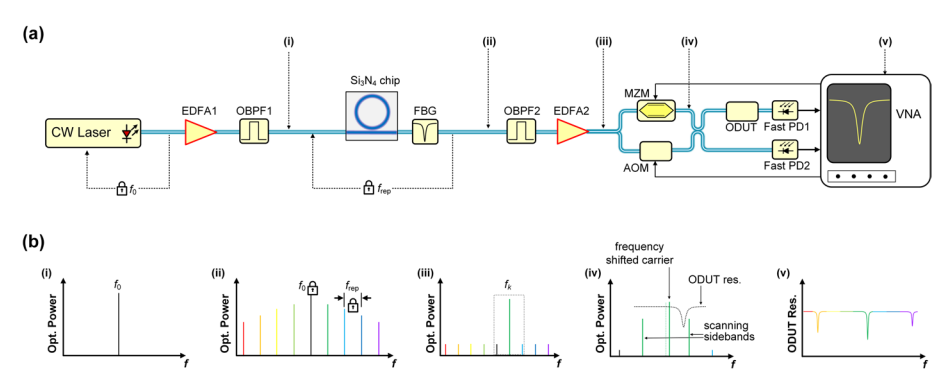


Fig. 1 Schematic diagram of miniaturized soliton-based high-accuracy broadband spectrometer. (a) The conceptual setup of the proposed spectrometer. f_0 : center frequency of the microcomb. $f_{\rm rep}$: repetition rate of the microcomb. CW laser: continuous-wave laser. PD: photodiode. EDFA: Erbium-doped fiber amplifier. OBPF: optical band-pass filter. FBG: fiber Bragg grating. MZM: Mach–Zehnder modulator. AOM: acousto-optic modulator. ODUT: optical device under test. VNA: vector network analyzer. (b) Optical and electrical signal evolution in the proposed spectrometer

Yang et al. PhotoniX (2025) 6:32 Page 4 of 14

microcomb spectrum exhibiting a flatness of 6.61 dB across the C-band is experimentally obtained, as shown in Fig. 2(a). The single-soliton state is achieved through the backward tuning technique [54]. The detuning is monitored by an additional VNA detecting the phase variance of the optical signal passing through the $\rm Si_3N_4$ micro-resonator. Figure 2(b) presents the microcomb stability diagram simulated by the Lugiato-Lefever equation (LLE). The microcomb system exhibits various regions with different stability properties, including modulation instability (MI), chaos (spatiotemporal chaos and transient chaos), breather, and stable solitons. By maintaining the pump power above the switching threshold $P_{\rm sw}$, and by electrical tuning the laser frequency and increasing the pump power several times, as shown in Fig. 2(b), the microcomb enters the chaos region, reducing the number of solitons one at a time until it transforms into a single-soliton state. Eventually, a flat sech²-shaped single-soliton microcomb spectrum with more than an 80 nm wavelength range is obtained, as depicted in Fig. 2(a).

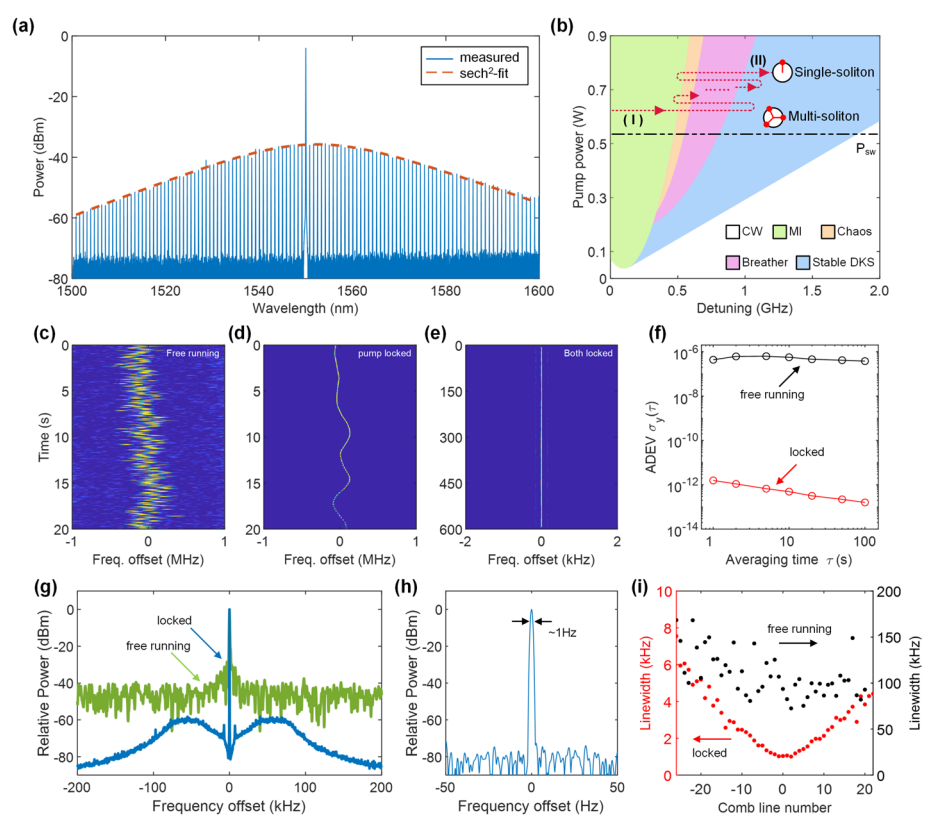


Fig. 2 Generation and stabilization of the single-soliton microcomb. (**a**) The optical spectrum of the experimentally generated single-soliton microcomb. (**b**) Simulated stability diagram of the soliton microcomb and the generation path of the single-soliton microcomb. Five different stability regions are listed: CW (white), modulation instability (MI, green), breather (magenta), spatio-temporal and transient chaos (chaos, yellow), and stable dissipative Kerr soliton (DKS, blue). The single-soliton microcomb is accessed above the switching threshold power by backward tuning and increasing pump power from a multi-soliton microcomb. (**c-e**) Spectrogram of in-loop repetition rate ($f_{\rm rep}$) of the free-running, pump-locked only, and fully locked soliton microcomb, respectively. (**f**) The overlapping Allan deviation of in-loop $f_{\rm rep}$ of the free-running and fully locked microcomb, respectively. (**g**) Electrical spectrum of in-loop $f_{\rm rep}$ of the fully locked microcomb. (**h**) The zoom-in spectrum of (**g**). (**i**) Measured linewidths of the comb lines of the soliton microcomb

Yang et al. PhotoniX (2025) 6:32 Page 5 of 14

The resolution and precision in frequency of the spectrometer largely depend on the stability and noise performance of the microcomb. The linewidth, namely the short-term stability of the comb line, directly determines the minimum resolution of the proposed spectrometer, as defined by the Rayleigh limit. The long-term drift of the wavelength of the comb lines can lead to frequency measurement errors. Additionally, data from one channel may overlap and interfere with those from other channels due to long-term drift. The optical frequency of the k_{th} comb line can be expressed as $f_k = f_0 + k \cdot f_{rep}$, where f_0 is the frequency of the pump laser, $f_{\rm rep}$ is the repetition rate. The stability of $f_{\rm rep}$ is crucial for the measurement precision of channels far from the center comb line, as the frequency of the k_{th} comb line drifts at least k times of f_{rep} . The stabilization of the pump laser is also essential. On one hand, the drift of f_0 contributes to the instability of all comb lines. On the other hand, the pump laser serves as one of the main noise sources of the soliton microcomb. Locking the pump laser to an ultra-stable laser can significantly improve the frequency stability of the pump laser itself as well as that of all comb lines. The details of frequency stabilization are as follows. First, the frequency of the pump laser is stabilized to an ultra-stable laser (Menlo ORS), using a PID controller (Toptica FALC 110) with a bandwidth of around few hundred kilohertz. The repetition rate of the soliton microcomb is stabilized using a second servo mechanism. The fluctuation of $f_{\rm rep}$ is optically frequency down-converted and then fed into a second FALC 110, which adjusts the pump power using an electrically tunable optical attenuator. Due to the nonlinear and thermo-refractive effects in the resonator, tuning the pump power alters the resonance frequency of the pumped mode and the laser detuning, thereby affecting f_{rep} . The bandwidth of the second servo is around 100 kHz, which is limited by the thermal response of the microresonator[12]. To further enhance the stabilities of the instruments, all microwave instruments in the locking scheme are referenced to the same rubidium atomic clock (Synchronization Technology Ltd. STW-FSJ2-RH-006) with an Allan deviation (ADEV) less than 1×10^{-12} at a 1-s averaging time.

Figures 2(c-e) depict the improvement in the stability of the repetition rate at each step of the locking process. The free-running $f_{\rm rep}$ experiences stochastic drifting caused by fluctuations in both the pump laser's power and frequency, with a maximum drift larger than 1 MHz. Initially, enabling the servo for the pump laser suppresses the fast-drifting components in $f_{\rm rep}$. However, slow-drifting components persist due to mechanical vibration of the coupling fiber. While the pump frequency is well-locked, fluctuations in pump power still affect the resonance frequency, causing a drift in $f_{\rm rep}$ of up to 218 kHz. These instabilities arise from the thermal and nonlinear effects of pump power fluctuations and residual detuning noise. Finally, engaging the second servo for $f_{\rm rep}$ and applying direct feedback processes significantly enhances $f_{\rm rep}$ stability, eliminating significant drift during the 600-s measurement. Another more accurate counter measurement demonstrates that compared to the free-running microcomb, a six-order magnitude improvement in the overlapping ADEV of the repetition rate can be observed as illustrated in Fig. 2(f). The overlapping ADEV reaches 1.56×10^{-12} at a 1-s and 1.59×10^{-13} at a 100s. The electrical spectra of the locked and free-running $f_{\rm rep}$ shown in Fig. 2(g) and (h) illustrate that the locked signal obtains a significant noise reduction, with a full-width half-maximum (FWHM) Linewidth of less than 1Hz. Taking into account the frequency stability of the atomic clock and the 150 mHz/s frequency drift of the ultra-stable laser,

Yang et al. PhotoniX (2025) 6:32 Page 6 of 14

the frequency drift of the outermost $-30_{\rm th}$ comb Line at 1525.4 nm, which exhibits the highest frequency instability used in the subsequent experiment, is calculated to be under 100 Hz over a 10-min period. The linewidths of the $-26_{\rm th}$ to $-22_{\rm nd}$ comb lines are measured using the self-heterodyne method. The free-running soliton microcomb's comb Line Linewidth can be as large as 168kHz, but after turning on the stabilization, the Linewidths significantly reduce, with the measured Linewidths now found to be less than 7.6 kHz. Higher-order comb lines cannot be measured due to their optical power falling below the measurement threshold. The linewidth of the $-30_{\rm th}$ comb Line is still estimated to be around 8.8 kHz, which remains sufficiently low for accurate measurements. The linewidths and stabilities of the comb lines can be further improved by using advanced locking techniques [56, 57].

Full C-band optical vector response measurement

The optical vector analysis is achieved through the utilization of the asymmetrical DSB method. The principle of the spectrometer is depicted in Fig. 1. The optical information of the entire measurement bandwidth is divided into multiple 103.9 GHz channels by the microcomb. The measurement is conducted channel by channel, and the results in each channel are combined after all channels are measured, as shown in Fig. 1(b). Though the frequency-stabilized soliton microcomb exhibits similar frequency stability to EOcombs [29, 58], the larger FSR of the soliton microcomb is more suitable for the spectrometer, particularly with channel bandwidths exceeding 100 GHz, resulting in fewer data needing digital compensation during channel switching. Both MZM (EOSPACE AX-0MVS-65) and PDs (Finisar XPDV3120R) exhibit good microwave response with reasonably large 3-dB bandwidths to handle the large channel spacing. Figure 1(a) illustrates the conceptual setup of the soliton microcomb-based spectrometer. To minimize the residual noise from adjacent channels and enhance the SNR of the system, two methods are employed. First, the flat spectrum of the soliton microcomb, with the pump line suppressed by an FBG, minimizes the possible unwanted spikes after optical filtering. Second, a high-extinction ratio optical filter (OBPF2, Santec OTF-980) is used for channel selection, further minimizing the residual noise from adjacent channels. As a result, the output optical signals from EDFA2 exhibit both high optical power and a high sidemode suppression ratio (SMSR); see the Supplemental Material for details. The optimization of optical power fed into EDFA2, achieved through a combination of OBPF2 with minimal insertion loss and soliton microcomb with a wide bandwidth, offers several advantages. It effectively increases the measurement bandwidth and enhances the SNR of received signals at the VNA, reducing the need for digital processing or averaging of multiple measurements. Consequently, it simultaneously enhances bandwidth, sensitivity, and measurement speed.

In each channel, the selected comb line from the $\mathrm{Si_3N_4}$ soliton microcomb is divided into two parts. One part is frequency-shifted to $f_k + \Delta f$ ($\Delta f = 80$ MHz) by an acousto-optic modulator (AOM) and serves as the optical carrier $E_{k, \mathrm{AOM}}(f)$. The other part passes through an MZM biased at the minimum transmission point, modulated by a frequency-sweeping RF signal (denoted as f_{e}) from the VNA (R&S ZVA67), generating a DSB signal $E_{k, \mathrm{DSB}}(f)$ with two sweeping optical sidebands at $f_k \pm f_{\mathrm{e}}$. $E_{k, \mathrm{AOM}}(f)$ and $E_{k, \mathrm{DSB}}(f)$ are then combined by a 2×2 optical coupler with their polarization aligned. The

Yang et al. PhotoniX (2025) 6:32 Page 7 of 14

two output asymmetrical DSB signals are respectively transmitted through the measurement path (including the ODUT) and the reference path, which can be mathematically expressed as:

$$\begin{cases}
E_{k,ref}(f) = \frac{E_{k,DSB}(f) + jE_{k,AOM}(f)}{\sqrt{2}} \\
E_{k,mea}(f) = \frac{jE_{k,DSB}(f) + E_{k,AOM}(f)}{\sqrt{2}} H_{DUT}(f)
\end{cases}$$
(1)

Here, $H_{\rm DUT}(f)$ represents the vector optical response to be recovered at frequency f. Then, the $\pm\,1_{\rm st}$ sidebands individually carry the amplitude and phase information of the ODUT. These signals are eventually detected by two fast PDs in both paths. The information carried by the $\pm\,1_{\rm st}$ sidebands is transformed into RF signals at $f_{\rm e}\pm\,\Delta f$, denoted as $i_{k,{\rm mea}}(f_{\rm e}\pm\,\Delta f)$ (from the measurement path), and $i_{k,{\rm ref}}(f_{\rm e}\pm\,\Delta f)$ (from the reference path), respectively. The VNA extracts the sideband frequencies via mixing and filtering, enabling vector optical response retrieval through comparison of the RF signals from both paths, as expressed by:

$$\begin{cases}
H(f_k - f_e) = \frac{i_{k,mea}(f_e + \triangle f)}{i_{k,ref}(f_e + \triangle f)jH^*(f_k + \triangle f)} \\
H(f_k - f_e) = \frac{i_{k,mea}(f_e - \triangle f)}{i_{k,ref}^*(f_e - \triangle f)j^*H(f_k + \triangle f)}
\end{cases}$$
(2)

By sweeping $f_{\rm e}$ from 0 to $f_{\rm rep}/2$, the complex optical spectrum within the frequency range from $f_{\rm k}$ — $f_{\rm rep}/2$ to $f_{\rm k}+f_{\rm rep}/2$ can be fully recovered. Consequently, the required 3-dB bandwidths of the MZM, PD, and VNA are reduced by half, to 51.95 GHz (i.e., 0.5×103.9 GHz). Furthermore, by sequentially measuring and stitching together the spectral responses associated with all comb lines, the complete spectrum spanning multiple free spectral ranges (FSRs) can be reconstructed.

In standard double sideband modulation, the beat note between the $1_{\rm st}$ and $2_{\rm nd}$ sidebands at the frequency of $f_{\rm e}$ introduces extra noise to the desired signal at $f_{\rm e}$, significantly degrading the SNR and dynamic range of the spectrometer. In our proposed spectrometer, however, the desired signals are carried by $f_{\rm e}\pm\Delta f$ frequencies, simplifying the filtering process for the interference signal at $f_{\rm e}$, as depicted in Fig. 1(c). Consequently, the proposed asymmetrical DSB method can simultaneously achieve a large dynamic range, large channel bandwidth, and high precision. A calibration process is employed to eliminate the response differences of the PDs by connecting the measurement path to the fast PD without passing through the ODUT. This enables the derivation of the calibration parameter $S_1 = S_{\rm mea1} \div S_{\rm ref1}$, where $S_{\rm mea1}$ and $S_{\rm ref1}$ represent responses obtained in each path, respectively. Upon inserting the ODUT, the measurement parameter $S_2 = S_{\rm mea2} \div S_{\rm ref2}$ is obtained. The final measurement result is calculated as $S_{\rm ODUT} = S_2 \div S_1$.

The transmission accuracy is validated by measuring the amplitude and group delay response of a H¹³C¹⁴N gas cell within a frequency range of 191.45 THz (1565.9 nm) to 196.33 THz (1527 nm), covering the entire optical C-band with a bandwidth of 4.88 THz (38.9 nm). With this step, the frequency of the spectrometer can be simultaneously calibrated to the absorption lines of the gas cell. Figure 3 compares the data from HITRAN2020 database [59] with measurements obtained using our proposed spectrometer and a commercially available spectrometer (Luna OVA 5000). The measured

Yang et al. PhotoniX (2025) 6:32 Page 8 of 14

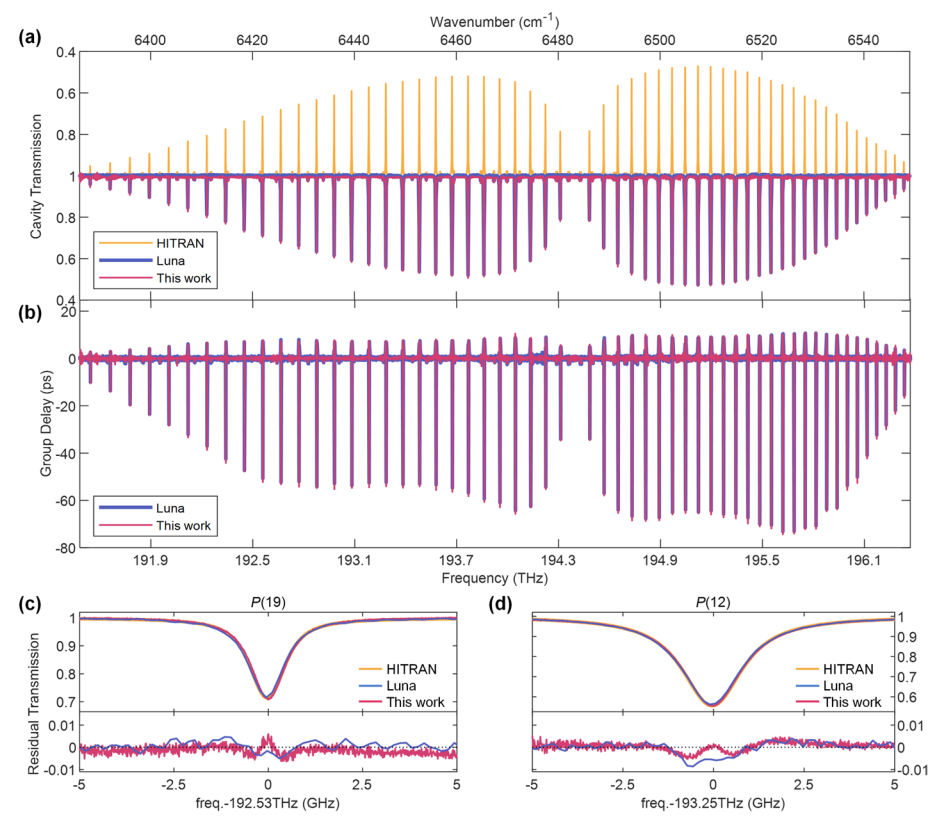


Fig. 3 Measurement results of the $H^{13}C^{14}N$ gas cell as the ODUT in the optical C band. Measured amplitude (a) and group delay (b) of the $H^{13}C^{14}N$ gas cell. The optical transmissions measured by the proposed spectrometer (red line) and by a commercial spectrometer (Luna OVA 5000, blue line) match well with the HITRAN2020 database (yellow line). The proposed spectrometer shows less fluctuation than the commercial spectrometer at the frequencies with no molecule absorption, indicating a better measurement sensitivity. (**c-d**) Details of the amplitude response of P(19) and P(12) lines of $H^{13}C^{14}N$ gas cell at 192.53 THz and 193.25 THz, respectively

transmissions differ slightly from the HITRAN simulation because the precise pressure of the gas cell is unknown. For the simulation, we used an estimated pressure of 18.7 Torr. The frequencies of the absorption lines of the gas cell measured by the proposed spectrometer perfectly align with the HITRAN data, demonstrating the good frequency stability of the comb lines acquired in the previous section. In most frequencies where no molecule absorption occurs, the proposed spectrometer produces similar or even slimmer horizontal lines than the commercial spectrometer in both amplitude and group delay responses. The thickness of the measured lines depends on the fluctuation of the measured data. The fluctuations are more prominent at the far ends of the frequency spectrum, both at the lowest and highest frequencies. This can be attributed to the fluctuation of the measured response depending on the microwave power received in the VNA. At both flanks of each channel of the spectrometer, MZM, fast PD1&2, and the VNA operate at very high frequencies, resulting in a large insertion loss for the received signal, thereby undermining the signal-to-noise ratio (SNR) of the received signal, which can also be observed in the residual of Fig. 3(d). Additionally, the EDFA exhibits a considerable performance reduction at the most marginal channels (1527 nm and 1565 nm). As a result, while spectra at these lower and higher frequencies are captured, the

Yang et al. PhotoniX (2025) 6:32 Page 9 of 14

absorption Lines are too weak to distinguish themselves from the data fluctuations of the two spectrometers. Although a resolution as high as $1 \,\mathrm{kHz}$ is achievable for our proposed spectrometer, it is unnecessary to use such a high resolution for measuring absorption Lines with a linewidth of Hundreds of megahertz. Thus, a resolution of $10 \,\mathrm{MHz}$ (0.08 pm) is selected as a trade-off for measurement speed. The frequency sweeping speed is approximately $10 \,\mathrm{GHz/s}$. Figure 3(c) compares the measured amplitude data for line P(19) from the gas cell. The absorption frequency obtained from the commercial spectrometer exhibits a deviation of about 50 MHz from the HITRAN data, attributed to its lower frequency measurement precision. Figures 3(d) presents the measured result of line P(12). The data measured by the commercial spectrometer is slightly distorted in the bottom part, and the absorption is slightly smaller than the HITRAN data. These results suggest that the measurement accuracy of the commercial spectrometer is limited by its low frequency resolution.

The results presented in Fig. 3 have already demonstrated the good performance of our proposed microcomb-based spectrometer. Nevertheless, they have not fully showcased the advantages of our spectrometer's high resolution and precision. The measurement of micro-resonators for optical frequency comb generation, on the other hand, necessitates a combination of wide bandwidth, high resolution, and high precision. This necessity arises because the Linewidths of resonances are less than 100MHz. Additionally, observing higher-order dispersion to predict the spectral locations of dispersive waves, which is crucial for designing an octave-spanning Kerr comb, requires a wide measurement range for accurate higher-order curve fitting. Traditionally, the use of wavelength scanning ECDLs results in deteriorated resonator dispersion measurement accuracy and increased system complexity [10-12, 16]. For the first time, we employ a soliton microcomb as the optical source for the microresonator dispersion measurement, eliminating the need for bulky and expensive ECDLs, thus reducing system complexity and enhancing accuracy. The measurement of integrated dispersion D_{int} , which is defined as $D_{int}(\mu) = \omega_{\mu} - (\omega_0 + D_1 \mu) = \frac{D_2}{2!} \mu^2 + \frac{D_3}{3!} \mu^3 + \frac{D_4}{4!} \mu^4 \dots$, is crucial for dispersion designing for microresonators, where ω_{μ} is angular frequency of the $\mu_{\rm th}$ mode, ω_0 is the center frequency for Taylor expansion, $D_1 = 2\pi \times FSR$, D_2 is the group delay dispersion (GVD), and D_3 , D_4 ... are higher-order dispersion coefficients. Since D_3 , D_4 are usually at least three orders of magnitude smaller than D_2 , a much wider dispersion measurement range is needed for accurate curve fitting.

Figure 4 presents the measurement result of a $\mathrm{Si_3N_4}$ micro-resonator. The proposed spectrometer can accurately measure the transmission spectrum due to the good stability of our comb lines and high measurement resolution. The integrated dispersion D_{int} and the linewidths of each resonance can be readily derived from the measured spectrum, as depicted in Figs. 4(b) and (d). By using Taylor expansion of the frequencies of the resonances at 1546 nm, we obtain that $D_1 = 2\pi \times 106.197$ GHz, $D_2 = 2\pi \times 12.164$ MHz. The Linewidths of the resonances obtained from the transmission spectrum are around 100MHz, which is comparable to the 100 MHz accuracy of a commercial wavelength meter used to calibrate the sweep nonlinearity of commercial lasers [60], and is approximately half the spectral resolution of the commercial spectrometer [61]. When measuring components with a linewidth similar to or smaller than the resolution, the measured spectrum is averaged in the frequency domain by the commercial

Yang et al. PhotoniX (2025) 6:32 Page 10 of 14

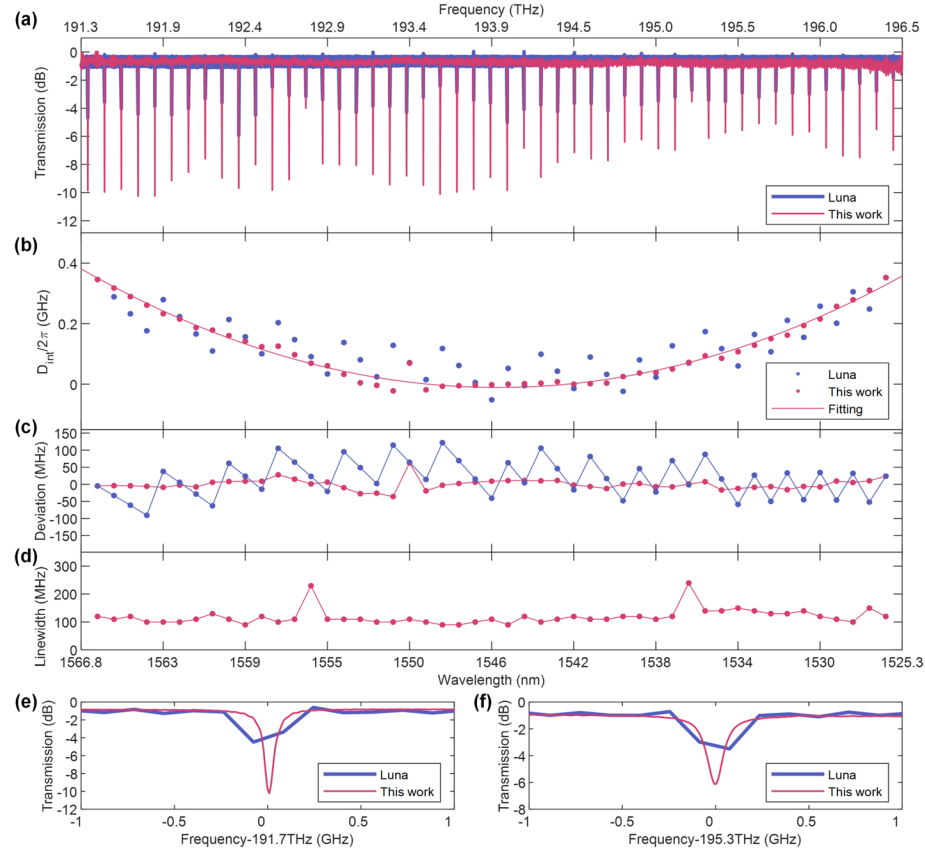


Fig. 4 Measurement results of a Si_3N_4 micro-resonator as the ODUT in the optical C band. (a) Optical transmission of the micro-resonator measured by the proposed spectrometer (red line) and a commercial spectrometer (Luna OVA 5000, blue line). The minimum optical transmission cannot be correctly measured because of its low resolution. (b) Measured dispersion of the micro-resonator. The integrated dispersion (D_{int}) curve (red line) is fit from the data measured by the proposed spectrometer in (a) (red dots). The frequencies of the resonances measured by the commercial spectrometer (blue dots) scatter far away from D_{int} curve due to its low frequency resolution. (c) Deviation between the D_{int} curve and the measured data in (b). (d) Linewidths of the resonances of the micro-resonator measured by the proposed spectrometer. (e), (f) Details of the optical transmission in (a) at 191.7 THz and 195.3 THz

spectrometer, resulting in distorted transmission spectra. Therefore, the transmission spectrum of all resonances measured by the commercial spectrometer is much shallower than the exact resonances, as shown in Fig. 4(a). Additionally, the frequencies of the resonances are not correctly measured, resulting in an oscillating quadratic curve in Figs. 4(b) and (c). Figures 4(e) and 4(f) present a comparison of two resonances measured by the two spectrometers. It is evident that the linewidths cannot be accurately obtained from the distorted spectra measured by the commercial spectrometer. In contrast, the high-resolution spectra provided by our proposed spectrometer Yield Linewidth measurements of 99.8 MHz and 139.7 MHz, respectively. The distortion in line-shape and the larger fluctuation in the horizontal parts of the spectra measured by the commercial spectrometer can be clearly observed. It should be noted that the measurement frequency range in Fig. 4 is from 191.3 THz (1566.8 nm) to 196.5 THz (1525.3 nm), corresponding to the $-19_{\rm th}$ and the $30_{\rm th}$ channel, respectively. The measurement bandwidth is 5.2 THz (41.5 nm), which is slightly larger than the measurement of the gas

Yang et al. PhotoniX (2025) 6:32 Page 11 of 14

cell because the absorption lines of the micro-resonator (about 10 dB) are significantly stronger than that of the gas cell (< 3 dB). The maximum operation frequency of OBPF2 is 196.58 THz (1525 nm), so higher frequencies are not measured. Frequencies lower than 191.3 THz (1566.8 nm) are not measured because the fluctuation rises rapidly, and it already exceeds the lower Limit frequency of the EDFA, which is 191.56 THz (1565 nm). In both cases, the measurement bandwidth surpasses the optical C band, i.e., the operational bandwidth of the EDFA, thus demonstrating the efficacy of our optimization approach for the spectrometer. If we can substitute EDFA2 with a C+L band EDFA, the bandwidth can be readily extended to 1625 nm. The proposed spectrometer offers excellent frequency stability, while the commercial spectrometer's frequency stability is Limited to around 1.5 pm due to its interferometric frequency calibration method. The commercial spectrometer's swept-frequency method and time-domain windowing for data analysis restrict its group delay precision to about 1 ps and its measurement range to 7 ns. In contrast, our spectrometer, based on a microwave photonics approach, provides superior performance in both aspects. The proposed spectrometer, with its wide bandwidth, high resolution, and high precision provided by the soliton microcomb, is a powerful tool for the dispersion design of high-Q micro-resonators, aiding in the guidance of optical Kerr frequency comb generation. Moreover, our work is highly valuable for various applications requiring precise dispersion engineering [6-9].

Conclusion

In summary, we present a miniaturized spectrometer utilizing only a GHz-tunable laser. The optical spectrum is broadened by a fully locked soliton microcomb, offering a remarkable frequency resolution of 1 kHz and an expansive measurement bandwidth of 5.2 THz (41 nm), effectively covering the entire optical C band. The measurement bandwidth is significantly improved by 650 times compared to the laser's electrical frequency tuning range. Notably, our proposed spectrometer holds promise for future advancements in bandwidth, frequency resolution, and measurement speed. In addition to measuring intensity transmission, the proposed spectrometer using microwave optical vector analyzing method can also characterize the phase response of the ODUT, enabling a comprehensive analysis of its complex transfer function and precise extraction of key parameters such as group delay, insertion loss, and dispersion. The demonstration of a spectrometer utilizing soliton microcomb generated on CMOS-compatible Si₃N₄ material represents a significant breakthrough, opening avenues for future chiplevel integration of spectrometers. Though the use of high-performance lasers in our work contributes to the overall system cost, this can be mitigated by adopting low-cost semiconductor diode lasers based on self-injection locking technique [55]. In addition, continued advances in chip fabrication technologies are expected to improve the yield and consistency of Si₃N₄-based soliton microcombs. This improvement, together with our demonstrated architecture, enables the seamless co-integration of various electrical or optical functionalities onto a single chip, including modulators [62], photodetectors [63, 64], reconfigurable optical filters [27, 65–70], and digital signal processors. Furthermore, the potential for heterogeneous or hybrid integration of additional devices such as lasers [71-73], AOMs [74], optical [75] and electrical amplifiers [76], and piezoelectric Yang et al. PhotoniX (2025) 6:32 Page 12 of 14

controllers [77] underscores the transformative impact of our work, laying a robust foundation for the realization of fully integrated spectrometers on the chip level.

Supplementary Information

The online version contains supplementary material available at https://doi.org/10.1186/s43074-025-00193-4.

Supplementary Material 1.

Acknowledgements

These authors contributed equally to this work.

Authors' contributions

H. Yang, H. Zhang, and Z. Ju implemented the generation and stabilization of soliton microcomb. H. Yang, X. Tang, H. Zhang, L. Wang carried out the spectra measurement and data analysis. H. Yang, Z. Kang, J. He, and S. Pan wrote the paper. J. He and S. Pan supervised the project.

Funding

This work was supported in part by the National Key Research and Development Program of China (2022YFB2802700); the National Natural Science Foundation of China (62205145, 62271249); the Natural Science Foundation of Jiangsu Province (BK20220887); Leading-Edge Technology Program of Jiangsu Natural Science Foundation (BK20232001).

Data availability

Data underlying the results presented in this paper are not publicly available at this time but may be obtained from the authors upon reasonable request.

Declarations

Ethics approval and consent to participate

Not applicable.

Consent for publication

Not applicable

Competing interests

Authors state no conflicts of interest.

Received: 10 October 2024 Revised: 6 August 2025 Accepted: 24 August 2025

Published online: 26 September 2025

References

- 1. Eriksson S, et al. Integrated optical components on atom chips. Eur Phys J D. 2005;35:135–9.
- 2. Savchenkov AA, et al. Kilohertz optical resonances in dielectric crystal cavities. Phys Rev A. 2004;70(5):051804.
- 3. Peng B, et al. Parity-time-symmetric whispering-gallery microcavities. Nat Phys. 2014;10:394–8.
- 4. Zhi Y, et al. Single nanoparticle detection using optical microcavities. Adv Mater. 2017;29:1604920.
- Endres CP, et al. The cologne database for molecular spectroscopy, CDMS, in the virtual atomic and molecular data centre, VAMDC. J Mol Spectrosc. 2016;327:95–104.
- 6. Woodward Rl. Dispersion engineering of mode-locked fibre lasers. J Opt. 2018;20(3):033002.
- 7. Li J, et al. Hybrid dispersion engineering based on chiral metamirror. Laser Photon Rev. 2023;17:2200777.
- 8. Guo H, et al. Mid-infrared frequency comb via coherent dispersive wave generation in silicon nitride nanophotonic waveguides. Nat Photon. 2018;12:330–5.
- Riemensberger J, et al. A photonic integrated continuous-travelling-wave parametric amplifier. Nature. 2022;612:56–61.
- Brasch V, et al. Photonic chip-based optical frequency comb using soliton cherenkov radiation. Science. 2016;351:357–60
- 11. Herr T, et al. Temporal solitons in optical microresonators. Nat Photonics. 2014;8:145–52.
- 12. Liu J, et al. High-yield, wafer-scale fabrication of ultralow-loss, dispersion-engineered silicon nitride photonic circuits. Nat Commun. 2021;12:2236.
- Zhang H, et al. Microresonator soliton frequency combs via cascaded Brillouin scattering. Commun Phys. 2025;8:216.
- Liu AQC, et al. Relative timing jitter compression in a Fabry–Pérot cavity-assisted free-running dual-comb interferometry. Adv Photon Nexus. 2024;3:056014.
- 15. Wan Z, et al. Quantum correlation-enhanced dual-comb spectroscopy. Light Sci Appl. 2025;14:257.
- Luo Y-H, et al. A wideband, high-resolution vector spectrum analyzer for integrated photonics. Light Sci Appl. 2024;13:83.
- 17. Xu B, et al. Whispering-gallery-mode barcode-based broadband sub-femtometer-resolution spectroscopy with an electro-optic frequency comb. Adv Photon. 2024;6:016006.

Yang et al. PhotoniX (2025) 6:32 Page 13 of 14

18. Gifford DK, et al. Optical vector network analyzer for single-scan measurements of loss, group delay, and polarization mode dispersion. Appl Opt. 2005;44:7282–6.

- Sagues M, Loayssa A. Swept optical single sideband modulation for spectral measurement applications using stimulated Brillouin scattering. Opt Express. 2010;18:17555–68.
- 20. Xue M, et al. Performance analysis of optical vector analyzer based on optical single-sideband modulation. Journal of the Optical Society of America B. 2013;30:928–33.
- 21. Wang WT, et al. Optical vector network analyzer with improved accuracy based on Brillouin-assisted optical carrier processing. IEEE Photonics J. 2014;6:1–10.
- 22. Feng H, et al. Integrated lithium niobate optical vector network analyzers based on single-sideband modulators, International Topical Meeting on Microwave Photonics (MWP). Nanjing: IEEE; 2023. p. 1–3.
- 23. Li W, et al. Optical vector network analyzer with improved accuracy based on polarization modulation and polarization pulling. Opt Lett. 2015;40:1679–82.
- 24. Wang M, Yao J. Optical vector network analyzer based on unbalanced double-sideband modulation. IEEE Photon Technol Lett. 2013;25:753–6.
- 25. Zou X, et al. Hyperfine intrinsic magnitude and phase response measurement of optical filters based on electro-optical harmonics heterodyne and Wiener-Lee transformation. J Lightwave Technol. 2019;37:2654–60.
- Zhang S, et al. On-the-fly precision spectroscopy with a dual-modulated tunable diode laser and Hz-level referencing to a cavity. Adv Photon. 2024;6:046003.
- 27. Marpaung D, et al. Integrated microwave photonics. Nat Photon. 2019;13:80–90.
- 28. Yao J, Capmany J. Microwave photonics. Sci China Inf Sci. 2022;65:221401.
- Qing T, et al. Optical vector analysis with attometer resolution, 90-dB dynamic range and THz bandwidth. Nat Commun. 2019;10:5135.
- Pfeiffer MHP, et al. Octave-spanning dissipative Kerr soliton frequency combs in Si₃N₄ microresonators. Optica. 2017;4:684–91.
- 31. Yi X, et al. Soliton frequency comb at microwave rates in a high-Q silica microresonator. Optica. 2015;2:1078-85.
- Kim S, et al. Dispersion engineering and frequency comb generation in thin silicon nitride concentric microresonators. Nat Commun. 2017;8:372.
- 33. Wang W, et al. Robust soliton crystals in a thermally controlled microresonator. Opt Lett. 2018;43:2002-5.
- 34. Shu H, et al. Microcomb-driven silicon photonic systems. Nature. 2022;605:457-63.
- 35. Marin-Palomo P, et al. Microresonator-based solitons for massively parallel coherent optical communications. Nature. 2017;546:274–9.
- Corcoran B, et al. Ultra-dense optical data transmission over standard fibre with a single chip source. Nat Commun. 2020:11:2568
- 37. Shao W, et al. Terabit FSO communication based on a soliton microcomb. Photonics Res. 2022;10:2802-8.
- 38. Suh MG, Vahala KJ. Soliton microcomb range measurement. Science. 2018;359:884–7.
- Wang JD, et al. Long-distance ranging with high precision using a soliton microcomb. Photonics Res. 2020;8:1964–72.
- Chen R, et al. Breaking the temporal and frequency congestion of LiDAR by parallel chaos. Nat Photon. 2023;17:306–14.
- 41. Suh MG, et al. Microresonator soliton dual-comb spectroscopy. Science. 2016;354:600-3.
- 42. Yang Q-F, et al. Vernier spectrometer using counterpropagating soliton microcombs. Science. 2019;363:965–8.
- 43. Wang Z, et al. Rhythmic soliton interactions for integrated dual-microcomb spectroscopy. 2024. arXiv:2402.08432.
- 44. Obrzud E, et al. A microphotonic astrocomb. Nat Photon. 2019;13:31-5.
- 45. Xu X, et al. 11 TOPS photonic convolutional accelerator for optical neural networks. Nature. 2021;589:44–51.
- 46. Wang X, et al. Chip-based high-dimensional optical neural network. Nano-Micro Lett. 2022;14:221.
- Hu JQ, et al. Reconfigurable radiofrequency filters based on versatile soliton microcombs. Nat Commun. 2020;11:4377.
- 48. Xu X, et al. Advanced RF and microwave functions based on an integrated optical frequency comb source. Opt Express. 2018;26:2569–83.
- 49. Yang H, et al. Fully programmable microwave photonic filter based on manageable two-soliton microcombs. J Lightwave Technol. 2023;41:7292–301.
- 50. Ding J, et al. Wideband image-reject RF channelization based on soliton microcombs (invited paper). APL Photon. 2023;8:090801.
- Liu JQ, et al. Photonic microwave generation in the X- and K-band using integrated soliton microcombs. Nat Photon. 2020;14(8):486.
- 52. Jin X., et al. Microresonator-referenced soliton microcombs with zeptosecond-level timing noise. 2024. arXiv:2401. 12760.
- 53. Lei F, et al. Optical linewidth of soliton microcombs. Nat Commun. 2022;13:3161.
- 54. Guo H, et al. Universal dynamics and deterministic switching of dissipative kerr solitons in optical microresonators. Nat Phys. 2017;13:94–102.
- 55. Pavlov NG, et al. Narrow-linewidth lasing and soliton Kerr microcombs with ordinary laser diodes. Nat Photon. 2018;12:694–8.
- 56. Niu R, et al. Atom-referenced and stabilized soliton microcomb. Sci China Phys Mech Astron. 2023;67:224262.
- 57. Li M, et al. Autonomous frequency locking for zero-offset microcomb. 2024. arXiv:2403.02868.
- 58. Zhang M, et al. Broadband electro-optic frequency comb generation in a lithium niobate microring resonator. Nature. 2019;568:373–7.
- Gordon IE, et al. The HITRAN2020 molecular spectroscopic database. J Quant Spectrosc Radiat Transfer. 2022:277:107949.
- Fujii S, Tanabe T. Dispersion engineering and measurement of whispering gallery mode microresonator for kerr frequency comb generation. Nanophotonics. 2020;9:1087–104.
- 61. "OVA 5100 Optical Vector Analyzer" (LUNA), http://lunainc.com/product/ova-5100.

Yang et al. PhotoniX (2025) 6:32 Page 14 of 14

- 62. Rahim A, et al. Taking silicon photonics modulators to a higher performance level: state-of-the-art and a review of new technologies. Adv Photon. 2021;3:024003–024003.
- 63. Michel J, et al. High-performance Ge-on-Si photodetectors. Nat Photon. 2010;4:527–34.
- 64. Shi Y, et al. 103GHz germanium-on-silicon photodiode enabled by an optimized U-shaped electrode. Photonics Res. 2024;12:1–6.
- 65. Miller DAB. Silicon photonics meshing optics with applications. Nat Photonics. 2017;11:403-4.
- 66. Pérez D, et al. Multipurpose silicon photonics signal processor core. Nat Commun. 2017;8:636.
- 67. Liu Y, et al. Integrated microwave photonic filters. Adv Opt Photon. 2020;12:485–555.
- 68. Zhang WF, Yao JP. Photonic integrated field-programmable disk array signal processor. Nat Commun. 2020;11:406.
- 69. Wu B, et al. Programmable integrated photonic coherent matrix: principle, configuring, and applications. Appl Phys Rev. 2024;11:011309.
- 70. Liu W, et al. A fully reconfigurable photonic integrated signal processor. Nat Photon. 2016;10:190-5.
- 71. Shen B, et al. Integrated turnkey soliton microcombs. Nature. 2020;582:365-9.
- 72. Wildi T, et al. Phase-stabilised self-injection-locked microcomb. Nat Commun. 2024;15:7030.
- 73. Xiang C, et al. Laser soliton microcombs heterogeneously integrated on silicon. Science. 2021;373:99–103.
- 74. Beller J, Shao L. Acousto-optic modulators integrated on-chip. Light Sci Appl. 2022;11:240.
- 75. Op de Beeck C, et al. Heterogeneous III-V on silicon nitride amplifiers and lasers via microtransfer printing. Optica. 2020;7:386–93.
- 76. Zhang G, et al. Hybrid-integrated wideband tunable optoelectronic oscillator. Opt Express. 2023;31:16929–38.
- 77. Liu J, et al. Monolithic piezoelectric control of soliton microcombs. Nature. 2020;583:385–90.

Publisher's Note

Springer Nature remains neutral with regard to jurisdictional claims in published maps and institutional affiliations.